Natural Hazards
and Earth System
Sciences

The ability of a stochastic regional weather generator to reproduce heavy-precipitation events across scales

Xiaoxiang Guan[1], **Viet Dung Nguyen**[1], **Paul Voit**[2], **Bruno Merz**[1,2], **Maik Heistermann**[2], **and Sergiy Vorogushyn**[1]

[1]GFZ Helmholtz Centre for Geosciences, Section Hydrology, Potsdam 14473, Germany
[2]Institute of Environmental Sciences and Geography, University of Potsdam, Potsdam 14476, Germany

Correspondence: Xiaoxiang Guan (guan@gfz.de)

Abstract. We assess the ability of a regional weather generator to represent the extremity of heavy-precipitation events (HPEs) across spatial and temporal scales. To this end, we implement a multi-site non-stationary regional weather generator (nsRWG) for the area of Germany and generate 100 sets of synthetic daily precipitation data spanning 72 years. The weather extremity index (WEI) and its recent cross-scale modification (xWEI) are applied to quantify the cross-scale extremity of synthetic and observed HPEs and to compare their distributions. The results show that the nsRWG excels in replicating the extremity patterns for almost all seven durations (ranging from 1 to 7 d) considered. The frequency of small-scale 1 d rainfall is, however, slightly overestimated. The nsRWG aptly reproduces the potential influential areas of HPEs, whether of a short or long duration. It is capable of generating precipitation events mirroring the extremity patterns observed during past disaster-causing HPEs in Germany, while simultaneously accommodating their variations. This study demonstrates the potential of the nsRWG for simulating HPE-related hazards and assessing flood risks.

1 Introduction

Heavy-precipitation events (HPEs) are rare weather phenomena which accumulate exceptional amounts of rainfall, within hours to days, over areas ranging from a few to tens of thousands of square kilometers. As the main cause of damaging floods and landslides, HPEs are the costliest natural disasters in Europe (Gvoždíková et al., 2019; NatCatSER-VICE, 2023; Swiss Re Institute, 2024). Climate change is expected to increase the frequency, intensity, and spatial ex-

tent of HPEs (Christensen and Christensen, 2003; Lenderink and Fowler, 2017; Matte et al., 2022; Yang et al., 2023) and their associated impacts (Merz et al., 2021).

Germany has experienced several notable HPEs in recent years (Hu and Franzke, 2020). For example, in August 2002, heavy precipitation led to record-high water levels in the Elbe River and its tributaries (Kreibich et al., 2017; Thieken et al., 2022). In July 2021, a widespread HPE hit the western and southern parts of Germany as well as neighboring countries and caused one of the most devastating flood events in German history, with more than 180 fatalities and EUR 33 billion in damages (Apel et al., 2022; Szönyi et al., 2022; Mohr et al., 2023).

To understand the physical mechanisms and to assess the potential consequences of HPEs, analyses of past events can be carried out (e.g., Caldas-Alvarez et al., 2022; Mohr et al., 2023). Alternatively, large ensembles of climate model simulations (e.g., Ehmele et al., 2022) or synthetic weather fields can be generated to extract a set of plausible HPEs. The latter option represents a more computationally efficient approach by deploying stochastic weather generators (WGs). WGs are stochastic models that are capable of generating synthetic spatiotemporal fields of weather variables such as precipitation, temperature, and humidity, retaining the statistical properties of observed or climate model data on which WGs are conditioned, such as autocorrelation, spatial covariance, and multi-variable dependence. A large number of WG models have been introduced so far, based on various statistical methods; among others, reshuffling and perturbing analogue weather fields or applying multi-variate autoregressive models (for a review, see Maraun et al., 2010; Haberlandt et al., 2011; Serinaldi and Kilsby, 2014; Benoit

and Mariethoz, 2017; Nguyen et al., 2021). WGs can be instrumental in generating synthetic HPEs, thereby supporting flood risk management and climate adaptation (Breinl et al., 2013; Chen and Brissette, 2014; Harris et al., 2014; Sairam et al., 2021). WGs are widely used for estimating hydrological design values (Winter et al., 2019), downscaling climate model output (Fatichi et al., 2011; Kiem et al., 2021), climate impact assessments on water resources (Harris et al., 2014; Najibi et al., 2024), and flood risk assessments (Sairam et al., 2021), providing long-term datasets for scenarios where observational data may be limited and where downscaled future climate projections are needed. WGs are particularly effective when integrated with other models to better understand and prepare for HPEs and their consequences (Mehrotra and Sharma, 2010; Zhou et al., 2020). For instance, long-term synthetic weather fields (like precipitation and air temperature) generated by WGs can be used as meteorological forcing for hydrological models in order to quantify HPE-related floods and damages (Apel et al., 2016; Qin and Lu, 2014; Sairam et al., 2021). This approach allows researchers to develop exceptional flood events needed for flood design or disaster management planning, as the generation of very long time series of flood flows and inundation increases the probability of obtaining situations where the unfortunate superposition of the different flood-generating processes leads to severe impacts (Falter et al., 2015). Such situations are rarely encountered in measured time series that are usually very limited in length.

Evaluating the performance of a WG is crucial to ensure that it accurately represents historical weather data and produces synthetic weather sequences that are adequate for the application context, e.g., flood estimation, drought assessment, climate change impact assessment (Tseng et al., 2020). The evaluation process helps to identify biases or limitations in the model output and fosters model improvements (e.g., Breinl et al., 2013; Serinaldi and Kilsby, 2014; Nguyen et al., 2021). Widely used metrics to evaluate synthetic precipitation data include the mean, standard deviation and skewness, lag-1 autocorrelation, frequency of wet (or dry) days, and precipitation intermittency (Steinschneider and Brown, 2013; Tseng et al., 2020; Zhou et al., 2020; Nguyen et al., 2021). Additionally, the performance of WGs in simulating the extremity of precipitation events is of special interest. The extremity of precipitation events is usually described by intensity, duration, and spatial extent statistics (Beniston and Stephenson, 2004; Jeferson de Medeiros et al., 2022; Müller and Kaspar, 2014; Zhang et al., 2011). The spatial consistency of multi-site WGs is sometimes evaluated based on the areal mean of the synthetic field within a region, e.g., the average rainfall of the catchment (Ullrich et al., 2021). However, this method may underrepresent the variability in the affected area, particularly when calculated in a fixed region, as the areal mean underestimates the extremity when only part of the region is heavily affected (Müller and Kaspar, 2014; Voit and Heistermann, 2022). To address these issues,

the correlation between multiple sites can be used to measure the spatial dependence structure of the precipitation amount across a region (Breinl et al., 2013; Gao et al., 2021; Tseng et al., 2020). Furthermore, the continuity ratio, expressed as the ratio between the average precipitation at one location when another location is dry or wet, can capture the spatial coherence of precipitation between adjacent locations (Wilks, 1998; Breinl et al., 2013). However, both the correlation coefficient and the spatial continuity ratio are dominated by the bulk of the precipitation events rather than by the extreme values.

HPEs can vary in duration, from short intense downpours to prolonged periods of heavy rainfall. Quantile-based thresholds of block maxima of precipitation totals and empirical probability distribution plots are typically used to characterize WG performance for extremes (Breinl et al., 2013; Zhou et al., 2020; Nguyen et al., 2021; Ullrich et al., 2021). Such methods are usually applied separately for different durations, neglecting the temporal coherence of HPEs, which in reality can be simultaneously extreme at different temporal and spatial scales, triggering different types of flooding overlaying each other (Ramos et al., 2017). For instance, during the 2002 Elbe flood, small-scale extreme precipitation caused flash floods in several small Elbe tributaries. During the same event, extreme rainfall over large spatial scales and longer durations triggered fluvial flooding, with widespread inundation and finally long-lasting groundwater flooding in the city of Dresden (Kreibich et al., 2005; Thieken et al., 2022). The ability of WGs to represent these cross-scale characteristics of precipitation events is thus essential for flood risk modeling. Up to now, no single measure has been used to evaluate the ability of WGs to capture the cross-scale extremity of rainfall.

In this study, we demonstrate a new evaluation approach for a WG based on the weather extremity index (WEI; Müller and Kaspar, 2014) and the cross-scale weather extremity index (xWEI) introduced by Voit and Heistermann (2022). These indices quantify the extremity of an event, considering different duration levels and spatial extents. xWEI additionally integrates the extremity over different duration levels and spatial extents. Our aim is to evaluate how well the cross-scale extremity of precipitation events is captured by a WG, even if it is not specifically tailored or trained to do so.

2 Study area and data

The study area is Germany (Fig. 1), given its exposure to hazards induced by heavy-precipitation events (HPEs), as highlighted in the introduction. A non-stationary regional weather generator (nsRWG) (Nguyen et al., 2024) is implemented for the whole of Germany and parts of the upstream neighboring countries, covering the five major river catchments – Elbe, Rhine, Danube, Ems, and Weser – to produce long-term spatially consistent synthetic precipitation and temperature data.
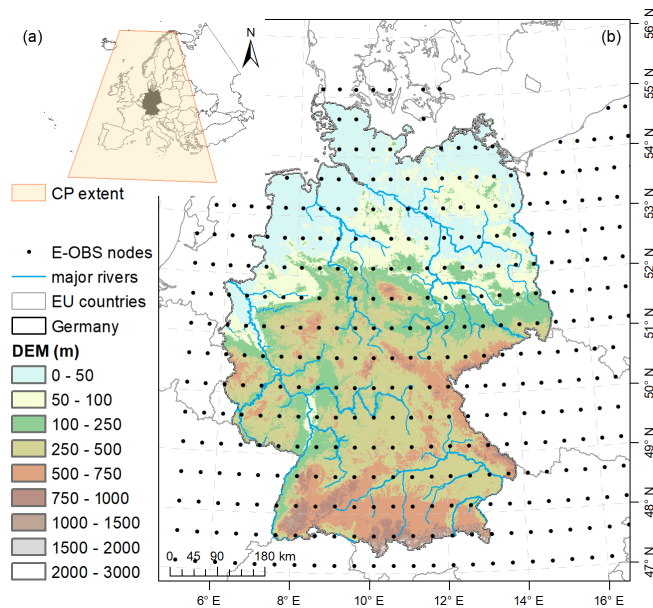
Figure 1. The study area (Germany and adjacent regions) and its topography, major rivers, and E-OBS grid nodes. The extent of where the mean sea level pressure was extracted to classify the circulation patterns (CPs) is shown in panel **(a)**.

In this study, we focus on the ability of the WG to represent the extremity of precipitation across scales. Weather generators that comprise several catchments and cover such a large spatial area (more than $650\,000\,\mathrm{km}^2$) are rare, and previous studies have commonly implemented WGs at smaller scales (Tseng et al., 2020; Ullrich et al., 2021; Gao et al., 2021).

Two datasets are used to parameterize the nsRWG: (1) gridded precipitation data from E-OBS (version 25.0e; Cornes et al., 2018) and (2) mean sea level pressure and daily air temperature at a 2 m height from the ERA5 reanalysis (Hersbach et al., 2020). Mean sea level pressure is used to classify circulation pattern types for which the local distributions of precipitation are conditioned. Regionally averaged daily temperature acts as a covariate of the local distribution in order to consider changes in precipitation for the same circulation pattern in a non-stationary warming world (Nguyen et al., 2024). Both the E-OBS and ERA5 datasets are available at a daily resolution, spanning from 1 January 1950 to 31 December 2021.

E-OBS is an ensemble gridded weather dataset and is available on a regular 0.25° grid, covering Europe. It is based on station data collated by the European Climate Assessment & Dataset initiative (Cornes et al., 2018). To cope with the high computational demands, we have resampled the grid points to a reduced spatial resolution of 0.5°. The locations of the extracted E-OBS grid points are given in Fig. 1.

The ERA5 dataset, provided by the European Centre for Medium-Range Weather Forecasts (ECMWF), is a state-of-the-art reanalysis dataset widely used in climate research

(Hersbach et al., 2020). It provides a comprehensive and detailed representation of atmospheric conditions at the global scale. To classify the large-scale atmospheric situation, mean sea level pressure is extracted over an extent (25–70° N, 15° W–30° E; see Fig. 1a) that encompasses a substantial portion of Europe and adjacent regions. The regional average 2 m daily air temperature is computed for the domain 45.125–55.125° N and 5.125–19.125° E, which covers the nsRWG setup area.

3 Methods

3.1 A stochastic multi-site non-stationary regional weather generator (nsRWG)

We adopt the non-stationary version of the multi-site regional weather generator nsRWG developed by Nguyen et al. (2024). The nsRWG represents the spatiotemporal dependence across sites using the first-order multi-variate autoregressive (MAR-1) model (Bardossy and Plate, 1992). The type-1 extended generalized Pareto (extGP) distribution is used to model daily non-zero precipitation amounts. This distribution is suitable not only for capturing both the lower bulk of precipitation amounts and the extreme values but also for providing a smooth transition along the precipitation range (Naveau et al., 2016; Nguyen et al., 2021).

In the nsRWG, the precipitation distribution at each site is conditioned on the large-scale circulation pattern as a latent variable and the regional average daily temperature as a covariate of the extGP distribution scale parameter. In this way, climate variability and climate change due to changes in dynamic and thermodynamic properties of the atmosphere are considered. Atmospheric circulation is classified into six circulation patterns based on mean sea level pressure for the winter (1 November–30 April) and summer (1 May–30 October) seasons (12 patterns in total). We use the objective classification algorithm Simulated ANnealing and Diversified RAndomization (SANDRA) based on the k-means clustering approach (Philipp et al., 2007) for circulation pattern classification. Further details about the nsRWG algorithm and configuration can be found in Nguyen et al. (2024).

The cross-scale precipitation performance of the nsRWG is evaluated for the E-OBS grid cells in the study area for the period from 1 January 1950 to 31 December 2021. We generate 100 realizations of synthetic precipitation datasets with a time series length of 72 years, corresponding to the length of the E-OBS dataset to ensure comparability.

3.2 WEI and xWEI

The weather extremity index (WEI) quantifies the extremity (a product of spatial extent and rarity) of an event, as well as the spatial extent and temporal duration at which the event reached its maximum extremity (Müller and Kaspar, 2014). In this context, the spatial extent of an event is not conceived

as an area of spatially contiguous grid cells but as a number of (potentially disjoint) cells in the study region (here, Germany) that exceeds a certain return period. The computation of WEI for individual HPEs is illustrated in Fig. 2. For a given spatial domain (in this case, Germany), it starts with the estimation of the return periods $P_{t,i}$ at each grid cell i for durations from 1 to t days. For each duration t, the grid cells in the spatial domain are sorted in decreasing order, based on their return period $P_{t,i}$ (in years) and then aggregated over increasing areas A (in km^2) by using Eq. (1): first, $E_{t,A}$ is computed for the most extreme grid cell ($n = 1$). Then, the following grid cells are added to the computation of $E_{t,A}$, increasing the value of n by 1 until the estimated return period from every grid cell is computed once. For each step, the area A equals the area of one single grid cell multiplied by n. In the final step, A corresponds to the size of the entire spatial domain. Finally, this procedure yields, for each duration t, a curve that shows $E_{t,A}$ as a function of A. The value of WEI is then defined by the maximum value of $E_{t,A}$ for all curves, and the spatial extent and duration at which the event was most extreme corresponds to the values of t and A, for which this maximum of $E_{t,A}$ is achieved. Note that the $E_{t,A}$ curves typically have a well-defined maximum: for low values of A, the steep increase of $\sqrt{A/\pi}$ (the radius of a circle of size A) causes an increase of $E_{t,A}$ with A. For larger values of A, the decrease in return periods dominates the behavior and causes the $E_{t,A}$ curve to decrease. The corresponding area where the $E_{t,A}$ curve reaches its peak (WEI) is denoted here as WEI area, which represents the spatial scale most severely affected by the HPE. The WEI area is always much smaller than the area over which the HPE precipitation totals exceed 0 mm. Rather, it is a weighted measure indicating the area in the domain that is heavily influenced by the HPE and hence prone to HPE-related impacts.

$$E_{t,A} = \frac{\sum_{i=1}^{n} \ln\left(P_{t,i}\right)}{n} \cdot \sqrt{A/\pi} \quad A = \text{grid size} \times n \quad (1)$$

As each $E_{t,A}$ curve represents how the extremity of an event extends across spatial scales, Voit and Heistermann (2022) proposed a cross-scale weather extremity index (xWEI) by integrating $E_{t,A}$ over duration ($\ln(t)$) and extent (A). xWEI quantifies how much the extremity of an event extends across both space and time (instead of the event just being extreme at one specific duration and extent). Hence, xWEI corresponds to the volume under the surface which is spanned by the $E_{t,A}$ curves (Fig. 2f) and placed on a grid:

$$\text{xWEI} = \int \int E_{t,A} \mathrm{d}A \mathrm{d}(\ln(t)). \quad (2)$$

For the exemplary HPE shown in Fig. 2, the analysis highlights the fact that the daily extremity (in terms of 1 d rainfall intensity) occurs on the fourth day, with the highest $E_{t,A}$ curve among the 7 d (Fig. 2d). Comparing extremity across

durations, the HPE is most extreme for a 1 d duration, affecting an area of over 10 000 km^2 (WEI area). For longer durations (≥ 3 d), the HPE consistently is extreme approximately for the same areas, showing a stabilization in spatial extent for these durations.

To estimate the return periods required to obtain $E_{t,A}$, we use the generalized extreme value (GEV) distribution, which has been found suitable for modeling precipitation extremes (Fowler and Kilsby, 2003) and has also been used in previous WEI studies (Gvoždíková et al., 2019; Minářová et al., 2018; Müller and Kaspar, 2014). The computation of xWEI requires return periods for multiple durations (1 to 7 d in our case). We use the duration-dependent GEV (dGEV) method (Koutsoyiannis et al., 1998) to estimate the return periods consistently across durations for each grid cell. Previous studies have shown that this method preserves the tail behavior of precipitation extremes across durations and modifies the scale and location parameters of the GEV distribution to explicitly account for dependency on the duration of events. This allows for more accurate modeling of precipitation intensity–duration–frequency relationships and reduces the uncertainty (Ulrich et al., 2020; Fauer et al., 2021). The parameters of the dGEV distribution at each grid cell are obtained by maximum likelihood estimation using the R package IDF (Ulrich et al., 2021) based on the annual maximum series of rainfall across considered durations.

To assess the extremity of HPEs across Germany, durations from 1 to 7 d are selected, as they are sufficient in capturing the events responsible for disastrous flood damage in the region (Ganguli and Merz, 2019). While WEI and xWEI can be extended to sub-daily scales (Voit and Heistermann, 2022), this analysis is conducted at the daily scale due to the limited availability of sub-daily precipitation observations. Additionally, short-duration high-intensity precipitation events usually affect comparatively small areas, whereas multi-day HPEs span larger regions and are more relevant for this study (Lengfeld et al., 2019, 2021; Orlanski, 1975).

The most extreme HPEs for these seven durations across Germany are identified by extracting the annual maximum WEI values for each duration based on E-OBS precipitation data for the historical period 1950–2021. The corresponding WEI areas (the area where the $E_{t,A}$ curve reaches its peak WEI) of the most extreme HPEs annually for each duration are categorized into six classes (Fig. 3) in order to analyze the spatial properties of HPEs in Germany. The same procedure is carried out for each of the 100 realizations to evaluate the performance of the nsRWG in reproducing the cross-scale properties of HPEs in Germany.
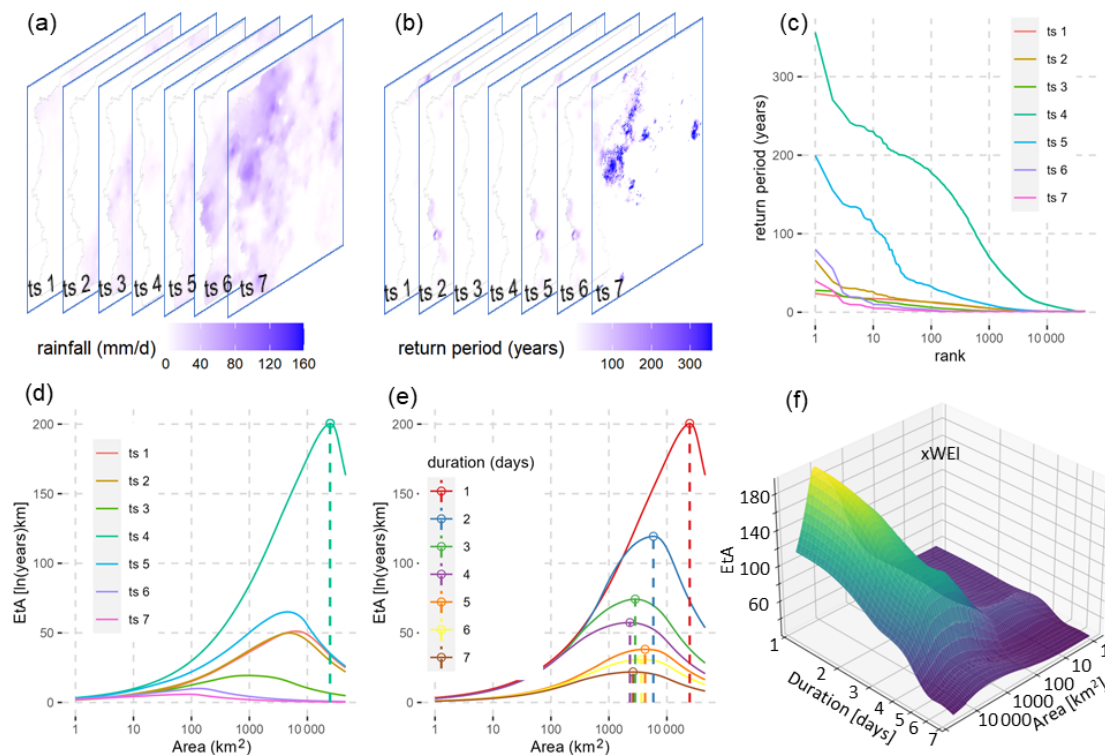
Nat. Hazards Earth Syst. Sci., 25, 3075–3086, 2025

https://doi.org/10.5194/nhess-25-3075-2025

Figure 2. Calculation of the WEI and xWEI for an exemplary HPE: **(a)** maps of daily rainfall for a precipitation event lasting 7 d, **(b)** return period at each individual grid cell of each map, **(c)** sorting of the return period estimates for each duration in decreasing order for each map, **(d)** calculation of the $E_{t,A}$ curves and selection of the curve with the highest peak to represent the extremity pattern of the precipitation for the duration of 1 d, **(e)** repetition of the procedures **(a–d)** for other durations (2, 3,…, 7 d) to derive the $E_{t,A}$ curves, and **(f)** 3D interpolated surface of $E_{t,A}$ for all durations and extents. xWEI is defined as the volume beneath the $E_{t,A}$ surface.

4   Results and discussion

4.1   nsRWG performance for WEI

Figure 3 shows the frequency distribution of the observed (E-OBS) and simulated (nsRWG) WEI areas of the annual maximum HPEs for seven different durations. The distributions of the annual maximum WEI values are given in Fig. 4. The results show that more than half of the annual maximum HPEs in Germany are events with WEI areas $\leq 20 \times 10^3$ km^2 for all durations. HPEs with a larger spatial extent of 20×10^3 km^2 or more have a frequency of less than 20 % in the past 72 years. However, these events are the most severe ones regarding their WEI values (Fig. 4). The nsRWG is able to reproduce the annual maximum WEI and its corresponding areas for the seven durations. The boxplots in Figs. 3 and 4 show that the simulated distribution patterns are in good agreement with the E-OBS observations. However, for shorter durations (1 and 2 d), the frequencies of HPEs with WEI areas $\leq 20 \times 10^3$ km^2 are overestimated, while those with larger WEI areas are underestimated (Fig. 3). For durations of 3 d and longer, the observed and simulated HPE frequencies are more balanced.

The relation between the annual maximum WEI values and their return periods derived from the nsRWG data agrees well with the E-OBS observations for the seven durations (Fig. 5). This comparison confirms the ability of the nsRWG to simulate the occurrence probability of HPEs in Germany. The observed probability plots (red dots in Fig. 5) are well enclosed by the simulated ranges (shaded areas) from the nsRWG realizations. This is especially true for high-return periods, which demonstrates the good performance in simulating HPEs for different durations. For short durations and return periods of between 2 and about 10 years, as well as for durations longer than 4 d with return periods between 10 and 20 years, the nsRWG slightly underestimates the observed WEI. In contrast to traditional intensity-duration-frequency curves, there is no systematic difference between the empirical probability plots of the annual maximum WEI series of different durations, as the WEI is based on return periods rather than precipitation totals or averages. This makes the WEI comparable across temporal scales. For example, for HPEs with the same WEI values, the return period increases with duration. This indicates that the occurrence probability of an HPE with the same extremity becomes smaller with increasing duration.
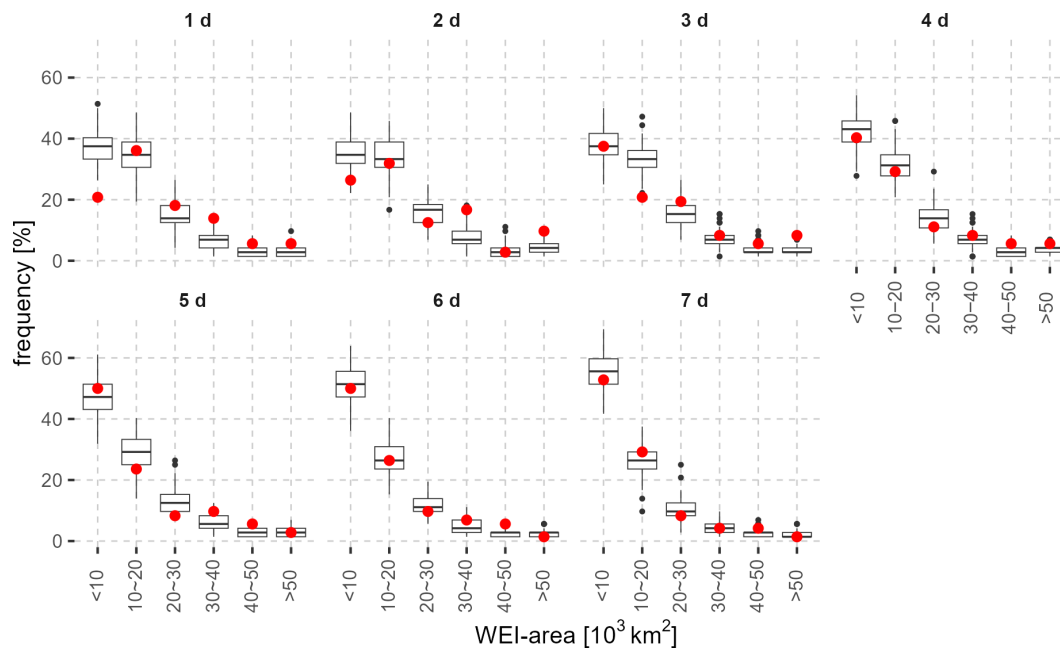
Figure 3. Frequency distribution of observed and nsRWG-simulated WEI areas of the annual maximum HPEs in the period 1950–2021 for seven durations. The titles of the subplots are the durations of interest. The red dots denote the frequency of HPEs in different area categories from E-OBS precipitation data, and the boxplots represent the simulated frequency distribution from the 100 nsRWG realizations.
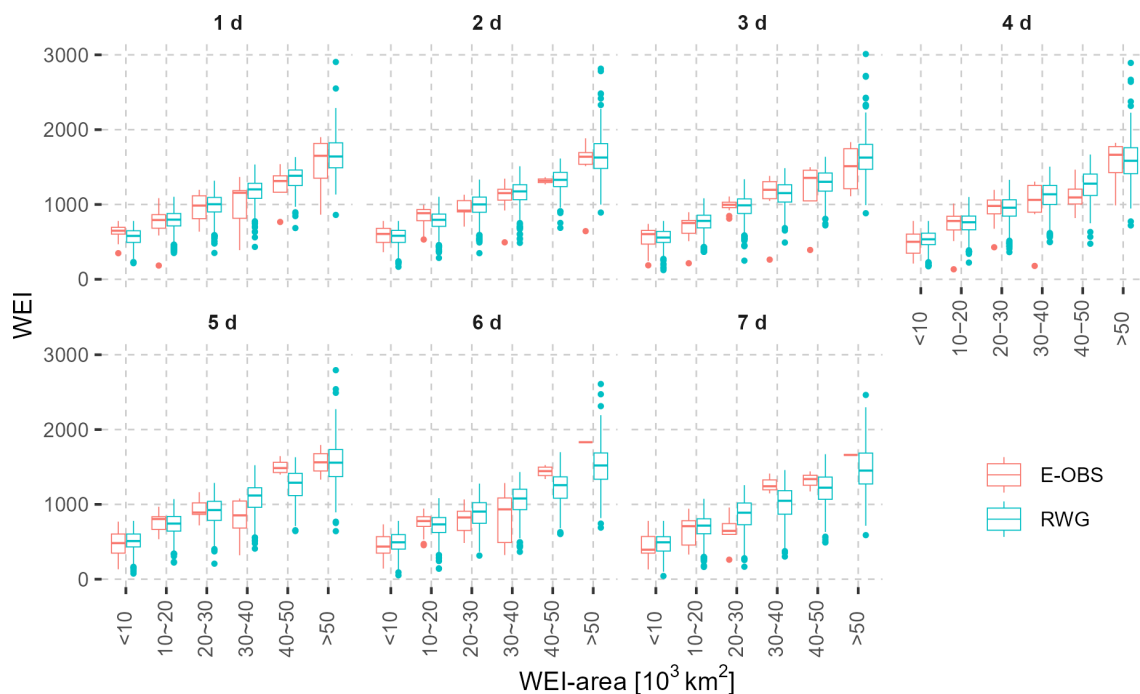

Figure 4. Distribution patterns of observed (red) and nsRWG-simulated (blue) annual maximum WEI series (denoted in the y axis, with the same unit as $E_{t,A}$: ln(years) · km) for seven durations. The WEI areas of HPEs are categorized into six classes (see the x axis).
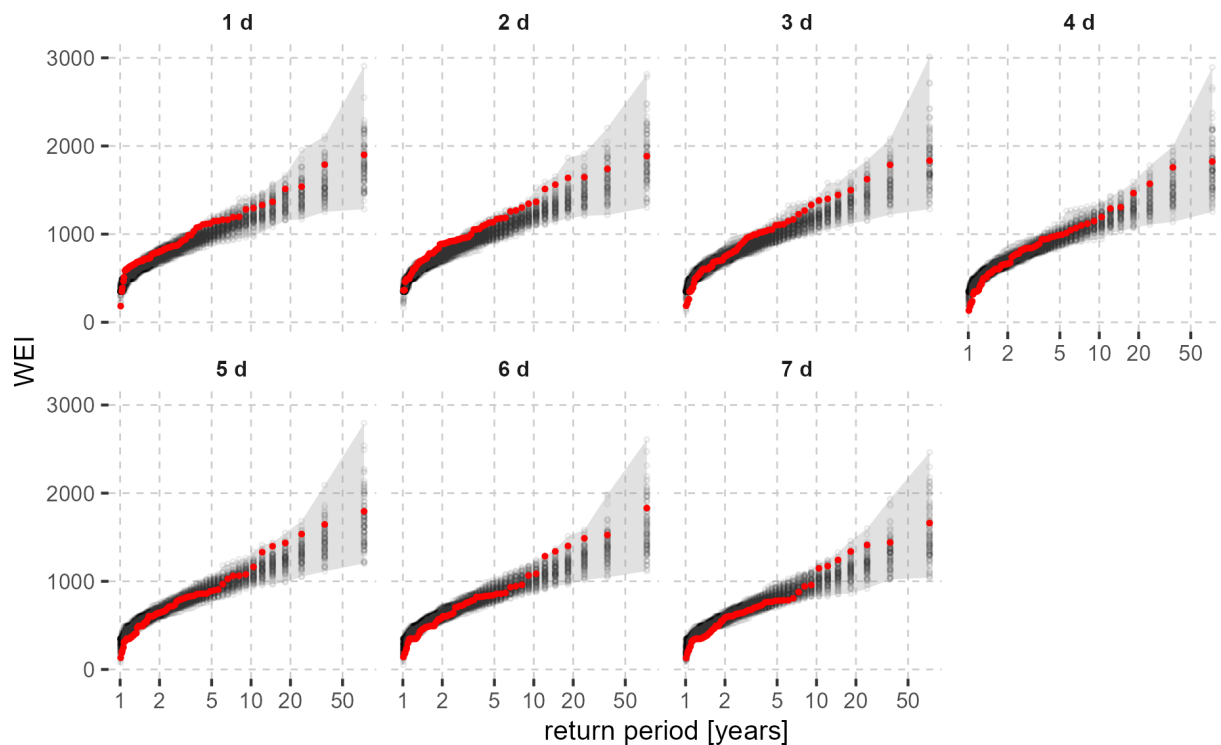
Figure 5. Empirical probability plots of E-OBS observed (red dots) and nsRWG-simulated (black dots) annual maximum WEI for seven durations. The Weibull plotting positions (Makkonen, 2006) are used to estimate the return periods. The gray shaded areas indicate the upper and lower boundaries of the nsRWG simulations.

4.2 nsRWG performance for xWEI

We compute the xWEI for HPEs in Germany for the period 1950–2021 and extract the annual maximum series from both the E-OBS dataset and the nsRWG realizations. The empirical probability plots of annual maximum xWEI, based on Weibull plotting positions (Makkonen, 2006), agree well for both datasets: the cross-scale extremity index xWEI of the observed data lies within the range of the 100 realizations (Fig. 6). However, for return periods between 2 and 5 years, the realizations of the nsRWG tend to underestimate the xWEI, similar to the performance of the WEI.

Figure 7 shows the extremity pattern of a real HPE in August 2002 – one of the most damaging events in Germany. In addition, HPEs from the nsRWG realizations with similar xWEI values to the August 2002 HPE are shown. Fig. 7b demonstrates that the nsRWG is able to generate HPEs with spatial and temporal extremity patterns that are very similar to the August 2002 event, characterized by the highest extremity for the durations of 1 and 2 d and an affected area of approximately 20 000 km². The other two nsRWG-generated HPEs with xWEI values similar to the August 2002 event show different cross-scale extremity patterns (emphasis on longer durations of 3–4 d). The reproducibility of historical HPEs illustrates the ability of the nsRWG in representing the cross-scale extremity of HPEs in Germany. The variations
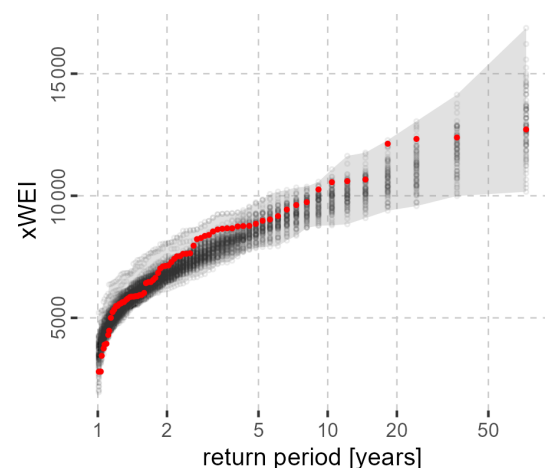

Figure 6. Empirical probability plots of observed (E-OBS, red dots) and simulated (nsRWG, black dots) annual maximum xWEI. The Weibull plotting position is used to estimate the empirical return periods. The gray shaded area indicates the upper and lower boundary of simulated xWEI from the 100 nsRWG realizations.

in synthetic events and the respective $E_{t,A}$ surfaces further demonstrate how the nsRWG can generate synthetic events, which are similar in terms of their cross-scale extremity but have their emphasis at different spatial and temporal scales.
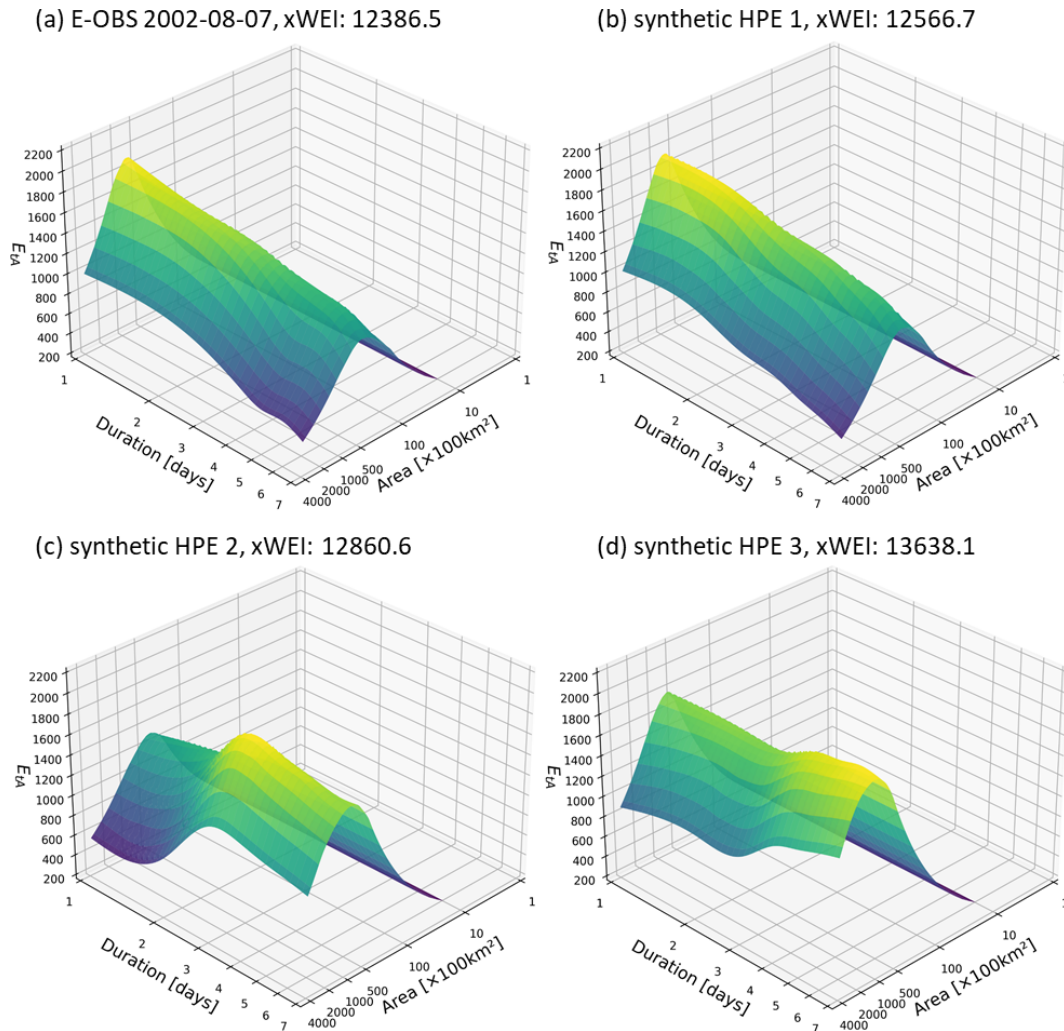
Figure 7. Cross-scale extremity pattern (interpolated $E_{t,A}$ curves over duration and area) of HPEs for **(a)** the August 2002 event and **(b–d)** three HPEs with similar xWEI values generated by the nsRWG. The HPE in panel **(b)** shows great similarity in the cross-scale extremity pattern with the August 2002 event in panel **(a)**, while the HPEs in panels **(c)** and **(d)** display different extremity patterns, although their xWEI values are similar to the actual event in August 2002.

5   Conclusions

In this study, we evaluate the ability of a multi-site stochastic regional weather generator to capture the extremity of HPEs across spatial and temporal scales. For this purpose, we set up the nsRWG at a large scale (covering all of Germany and riparian regions) and generate 100 realizations of 72 years of synthetic precipitation data at a daily resolution. The performance evaluation of the nsRWG in simulating precipitation focuses on the event scale and extreme cases. This focus complements typical proxy statistics (like mean and standard deviation) that tend to represent only the general properties of WGs in precipitation generation. Two indices, WEI and xWEI, are used to measure the extremity of observed and synthetic HPEs, both of them based on the spatial aggregation of return periods of precipitation totals for several du-

rations of interest. While WEI quantifies the maximum extremity of an event that occurred at a specific spatial extent and temporal duration, xWEI integrates extremity across the spatial and temporal scales of interest. The results demonstrate that the nsRWG performs well in simulating the extremity patterns across most spatial and temporal scales of HPEs in Germany. However, it tends to overestimate the frequency of events with short durations and relatively small spatial extents. Using the August 2002 event as an example, we illustrate how the nsRWG is able to generate precipitation events with spatiotemporal extremity patterns similar to those of historical disaster-causing HPEs.

With regard to future research, we emphasize that the choice of the spatial domain at which WGs are evaluated (here, all of Germany) is always a trade-off: on the one hand, the impacts of HPEs unfold at the catchment scale, and it

would be an obvious next step to evaluate the ability of the WG to reproduce the frequencies of WEI and xWEI occurrence at the scale of specific river catchments (at the cost of computational effort, as this would require a higher spatial resolution). On the other hand, we need to be aware that an HPE that occurred in one catchment may potentially also occur in a neighboring catchment, so that an analysis at a larger spatial domain (than the present one) is certainly warranted. Such considerations also show the links to "spatial counterfactuals", which have recently gained attention (Merz et al., 2024; Voit and Heistermann, 2024; Vorogushyn et al., 2025). Counterfactuals are scenarios that describe alternative ways of how an event could have unfolded (Woo, 2019; Montanari et al., 2024). These scenarios could involve conditions where specific factors, such as anthropogenic climate change, natural climate variability, or other boundary conditions, are altered or removed (Gauch et al., 2020). Spatial counterfactuals are a special case of counterfactual scenarios that consider the transposition of hazard characteristics e.g., precipitation in space. Using spatial counterfactual scenarios, we can investigate the impact of HPEs in the hypothetical case that they had happened elsewhere. Weather generators could be a useful tool in exploring how events with similar extremity indices could unfold in different locations of the spatial domain or with different spatiotemporal signatures, hence supporting the evaluation of counterfactual scenarios.

Author contributions. XG: data curation, conceptualization, methodology, formal analysis, visualization, and writing (original draft preparation). VDN: data curation, methodology, and software. PV: methodology, software, and writing (review and editing). BM: supervision and writing (review and editing). MK: writing (review and editing). SV: conceptualization, supervision, and writing (original draft preparation).

Disclaimer. Publisher's note: Copernicus Publications remains neutral with regard to jurisdictional claims made in the text, published maps, institutional affiliations, or any other geographical representation in this paper. While Copernicus Publications makes every effort to include appropriate place names, the final responsibility lies with the authors.

References

Apel, H., Martínez Trepat, O., Hung, N. N., Chinh, D. T., Merz, B., and Dung, N. V.: Combined fluvial and pluvial urban flood hazard analysis: concept development and application to Can Tho city, Mekong Delta, Vietnam, Nat. Hazards Earth Syst. Sci., 16, 941–961, https://doi.org/10.5194/nhess-16-941-2016, 2016.

Apel, H., Vorogushyn, S., and Merz, B.: Brief communication: Impact forecasting could substantially improve the emergency management of deadly floods: case study July 2021 floods in Germany, Nat. Hazards Earth Syst. Sci., 22, 3005–3014, https://doi.org/10.5194/nhess-22-3005-2022, 2022.

Bardossy, A. and Plate, E. J.: Space-time model for daily rainfall using atmospheric circulation patterns, Water Resour. Res., 28, 1247–1259, https://doi.org/10.1029/91WR02589, 1992.

Beniston, M. and Stephenson, D. B.: Extreme climatic events and their evolution under changing climatic conditions, Global Planet. Change, 44, 1–9, https://doi.org/10.1016/j.gloplacha.2004.06.001, 2004.

Benoit, L. and Mariethoz, G.: Generating synthetic rainfall with geostatistical simulations, WIREs Water, 4, e1199, https://doi.org/10.1002/wat2.1199, 2017.

Breinl, K., Turkington, T., and Stowasser, M.: Stochastic generation of multi-site daily precipitation for applications in risk management, J. Hydrol., 498, 23–35, https://doi.org/10.1016/j.jhydrol.2013.06.015, 2013.

Caldas-Alvarez, A., Augenstein, M., Ayzel, G., Barfus, K., Cherian, R., Dillenardt, L., Fauer, F., Feldmann, H., Heistermann, M., Karwat, A., Kaspar, F., Kreibich, H., Lucio-Eceiza, E. E., Meredith, E. P., Mohr, S., Niermann, D., Pfahl, S., Ruff, F., Rust, H.

W., Schoppa, L., Schwitalla, T., Steidl, S., Thieken, A. H., Tradowsky, J. S., Wulfmeyer, V., and Quaas, J.: Meteorological, impact and climate perspectives of the 29 June 2017 heavy precipitation event in the Berlin metropolitan area, Nat. Hazards Earth Syst. Sci., 22, 3701–3724, https://doi.org/10.5194/nhess-22-3701-2022, 2022

Chen, J. and Brissette, F. P.: Stochastic generation of daily precipitation amounts: review and evaluation of different models, Clim. Res., 59, 189–145, https://doi.org/10.3354/cr01214, 2014.

Christensen, J. H. and Christensen, O. B.: Severe summertime flooding in Europe, Nature, 421, 805–806, https://doi.org/10.1038/421805a, 2003.

Cornes, R. C., van der Schrier, G., van den Besselaar, E. J. M., and Jones, P. D.: An Ensemble Version of the E-OBS Temperature and Precipitation Data Sets, J. Geophys. Res.-Atmos., 123, 9391–9409, https://doi.org/10.1029/2017JD028200, 2018.

ECAD: European Climate Assessment and Dataset project: E-OBS gridded precipitation and temperature data, https://surfobs.climate.copernicus.eu/dataaccess/access_eobs.php#datafiles (last access: 23 June 2025), Copernicus Climate Data Store [data set], 2025.

Ehmele, F., Kautz, L.-A., Feldmann, H., He, Y., Kadlec, M., Kelemen, F. D., Lentink, H. S., Ludwig, P., Manful, D., and Pinto, J. G.: Adaptation and application of the large LAERTES-EU regional climate model ensemble for modeling hydrological extremes: a pilot study for the Rhine basin, Nat. Hazards Earth Syst. Sci., 22, 677–692, https://doi.org/10.5194/nhess-22-677-2022, 2022.

Falter, D., Schröter, K., Dung, N. V., Vorogushyn, S., Kreibich, H., Hundecha, Y., Apel, H., and Merz, B.: Spatially coherent flood risk assessment based on long-term continuous simulation with a coupled model chain, J. Hydrol., 524, 182–193, https://doi.org/10.1016/j.jhydrol.2015.02.021, 2015.

Fatichi, S., Ivanov, V. Y., and Caporali, E.: Simulation of future climate scenarios with a weather generator, Adv. Water Resour., 34, 448–467, https://doi.org/10.1016/j.advwatres.2010.12.013, 2011.

Fauer, F. S., Ulrich, J., Jurado, O. E., and Rust, H. W.: Flexible and consistent quantile estimation for intensity–duration–frequency curves, Hydrol. Earth Syst. Sci., 25, 6479–6494, https://doi.org/10.5194/hess-25-6479-2021, 2021.

Fowler, H. J. and Kilsby, C. G.: A regional frequency analysis of United Kingdom extreme rainfall from 1961 to 2000, Int. J. Climatol., 23, 1313–1334, https://doi.org/10.1002/joc.943, 2003.

Ganguli, P. and Merz, B.: Extreme Coastal Water Levels Exacerbate Fluvial Flood Hazards in Northwestern Europe, Scientific Reports, 9, 1–14, https://doi.org/10.1038/s41598-019-49822-6, 2019.

Gao, C., Guan, X. J., Booij, M. J., Meng, Y., and Xu, Y. P.: A new framework for a multi-site stochastic daily rainfall model: Coupling a univariate Markov chain model with a multi-site rainfall event model, J. Hydrol., 598, 126478, https://doi.org/10.1016/j.jhydrol.2021.126478, 2021.

Gauch, M., Klotz, D., Kratzert, F., Nearing, S., Hochreiter, S., and Lin, J.: A Machine Learner's Guide to Streamflow Prediction, in: Workshop on AI for Earth Sciences 34th Conference on Neural Information Processing Systems (NeurIPS 2020), Vancouver, Canada, 12 December 2020, https://cs.uwaterloo.ca/~jimmylin/publications/ 2020.

Gvoždíková, B., Müller, M., and Kašpar, M.: Spatial patterns and time distribution of central European extreme precipitation events between 1961 and 2013, Int. J. Climatol., 39, 3282–3297, https://doi.org/10.1002/joc.6019, 2019.

Haberlandt, U., Hundecha, Y., Pahlow, M., and Schumann, A. H.: Rainfall generators for application in flood studies, in: Flood Risk Assessment and Management, edited by: Schumann, A. H., Springer, Netherlands, 117–147, https://doi.org/10.1007/978-90-481-9917-4_7, 2011.

Harris, C. N. P., Quinn, A. D., and Bridgeman, J.: The use of probabilistic weather generator information for climate change adaptation in the UK water sector, Meteorol. Appl., 21, 129–140, https://doi.org/10.1002/met.1335, 2014.

Hersbach, H., Bell, B., Berrisford, P., Hirahara, S., Horányi, A., Muñoz-Sabater, J., Nicolas, J., Peubey, C., Radu, R., Schepers, D., Simmons, A., Soci, C., Abdalla, S., Abellan, X., Balsamo, G., Bechtold, P., Biavati, G., Bidlot, J., Bonavita, M., De Chiara, G., Dahlgren, P., Dee, D., Diamantakis, M., Dragani, R., Flemming, J., Forbes, R., Fuentes, M., Geer, A., Haimberger, L., Healy, S., Hogan, R.J., Hólm, E., Janisková, M., Keeley, S., Laloyaux, P., Lopez, P., Lupu, C., Radnoti, G., de Rosnay, P., Rozum, I., Vamborg, F., Villaume, S., and Thépaut, J.-N.: The ERA5 global reanalysis, Q. J. Roy. Meteor. Soc., 146, 1999–2049, https://doi.org/10.1002/qj.3803, 2020.

Hersbach, H., Bell, B., Berrisford, P., Biavati, G., Horányi, A., Muñoz Sabater, J., Nicolas, J., Peubey, C., Radu, R., Rozum, I., Schepers, D., Simmons, A., Soci, C., Dee, D., and Thépaut, J.-N.: ERA5 hourly data on single levels from 1940 to present, Copernicus Climate Change Service (C3S) Climate Data Store (CDS) [data set], https://doi.org/10.24381/cds.adbb2d47, 2023.

Hu, G. and Franzke, C. L. E.: Evaluation of Daily Precipitation Extremes in Reanalysis and Gridded Observation-Based Data Sets Over Germany, Geophys. Res. Lett., 47, e2020GL089624, https://doi.org/10.1029/2020GL089624, 2020.

Jeferson de Medeiros, F., Prestrelo de Oliveira, C. and Avila-Diaz, A. Evaluation of extreme precipitation climate indices and their projected changes for Brazil: From CMIP3 to CMIP6. Weather and Climate Extremes, 38, 100511, https://doi.org/10.1016/j.wace.2022.100511, 2022.

Kiem, A. S., Kuczera, G., Kozarovski, P., Zhang, L., and Willgoose, G.: Stochastic generation of future hydroclimate using temperature as a climate change covariate, Water Resour. Res., 57, 2020WR027331, https://doi.org/10.1029/2020WR027331, 2021.

Koutsoyiannis, D., Kozonis, D., and Manetas, A.: A mathematical framework for studying rainfall intensity-duration-frequency relationships, J. Hydrol., 206, 118–135, https://doi.org/10.1016/S0022-1694(98)00097-3, 1998.

Kreibich, H., Petrow, T., Thieken, A. H., Müller, M., and Merz, B.: Consequences of the extreme flood event of August 2002 in the city of Dresden, Germany, in: Sustainable Water Management Solutions for Large Cities, edited by: Savic, D. A., Mariño, M. A., Savenije, H. H. G., and Bertoni, J. C., IAHS Publication, 293, 164–173, 2005.

Kreibich, H., Di Baldassarre, G., Vorogushyn, S., Aerts, J. C. J. H., Apel, H., Aronica, G. T., Arnbjerg-Nielsen, K., Bouwer, L.M., Bubeck, P., Caloiero, T., Chinh, D.T., Cortès, M., Gain, A.K., Giampá, V., Kuhlicke, C., Kundzewicz, Z. W., Llasat, M. C., Mård, J., Matczak, P., Mazzoleni, M., Molinari, D., Dung, N.

Nat. Hazards Earth Syst. Sci., 25, 3075–3086, 2025

https://doi.org/10.5194/nhess-25-3075-2025

V., Petrucci, O., Schröter, K., Slager, K., Thieken, A. H., Ward, P. J., and Merz, B.: Adaptation to flood risk: Results of international paired flood event studies, Earth's Future, 5, 953–965, https://doi.org/10.1002/2017ef000606, 2017.

Lenderink, G. and Fowler, H. J.: Understanding rainfall extremes, Nat. Clim. Change, 7, 391–393, https://doi.org/10.1038/nclimate3305, 2017.

Lengfeld, K., Winterrath, T., Junghänel, T., Hafer, M., and Becker, A.: Characteristic spatial extent of hourly and daily precipitation events in Germany derived from 16 years of radar data, Meteorol. Z., 28, 363–378, https://doi.org/10.1127/metz/2019/0964, 2019.

Lengfeld, K., Walawender, E., Winterrath, T., and Becker, A.: CatRaRE: A Catalogue of radar-based heavy rainfall events in Germany derived from 20 years of data, Meteorol. Z., 30, 469–487, https://doi.org/10.1127/metz/2021/1088, 2021.

Makkonen, L.: Plotting Positions in Extreme Value Analysis, J. Appl. Meteorol. Clim., 45, 334–340, https://doi.org/10.1175/JAM2349.1, 2006.

Maraun, D., Wetterhall, F., Ireson, A. M., Chandler, R. E., Kendon, E. J., Widmann, M., Brienen, S., Rust, H. W., Sauter, T., Themel, M., Venema, V. K. C., Chun, K. P., Goodess, C. M., Jones, R. G., Onof, C., Vrac, M., and Thiele-Eich, I.: Precipitation downscaling under climate change: Recent developments to bridge the gap between dynamical models and the end user, Rev. Geophys., 48, RG3003, https://doi.org/10.1029/2009RG000314, 2010.

Matte, D., Christensen, J. H., and Ozturk, T.: Spatial extent of precipitation events: when big is getting bigger, Clim. Dynam., 58, 1861–1875, https://doi.org/10.1007/s00382-021-05998-0, 2022.

Mehrotra, R. and Sharma, A.: Development and Application of a Multisite Rainfall Stochastic Downscaling Framework for Climate Change Impact Assessment, Water Resour. Res., 46, W07526, https://doi.org/10.1029/2009WR008423, 2010.

Merz, B., Blöschl, G., Vorogushyn, S., Dottori, F., Aerts, J. C. J. H., Bates, P., Bertola, M., Kemter, M., Kreibich, H., Lall, U., and Macdonald, E.: Causes, impacts and patterns of disastrous river floods, Nature Reviews Earth & Environment, 2, 592–609, https://doi.org/10.1038/s43017-021-00195-3, 2021.

Merz, B., Nguyen, V. D., Guse, B., Han, L., Guan, X., Rakovec, O., Samaniego, L., Ahrens, B., and Vorogushyn, S.: Spatial counterfactuals to explore disastrous flooding, Environ. Res. Lett., 19, 044022, https://doi.org/10.1088/1748-9326/ad22b9, 2024.

Minářová, J., Müller, M., Clappier, A., and Kašpar, M.: Comparison of extreme precipitation characteristics between the Ore Mountains and the Vosges Mountains (Europe), Theor. Appl. Climatol., 133, 1249–1268, https://doi.org/10.1007/s00704-017-2247-x, 2018.

Mohr, S., Ehret, U., Kunz, M., Ludwig, P., Caldas-Alvarez, A., Daniell, J. E., Ehmele, F., Feldmann, H., Franca, M. J., Gattke, C., Hundhausen, M., Knippertz, P., Küpfer, K., Mühr, B., Pinto, J. G., Quinting, J., Schäfer, A. M., Scheibel, M., Seidel, F., and Wisotzky, C.: A multi-disciplinary analysis of the exceptional flood event of July 2021 in central Europe – Part 1: Event description and analysis, Nat. Hazards Earth Syst. Sci., 23, 525–551, https://doi.org/10.5194/nhess-23-525-2023, 2023.

Montanari, A., Merz, B., and Blöschl, G.: HESS Opinions: The sword of Damocles of the impossible flood, Hydrol. Earth Syst. Sci., 28, 2603–2615, https://doi.org/10.5194/hess-28-2603-2024, 2024.

Müller, M. and Kaspar, M.: Event-adjusted evaluation of weather and climate extremes, Nat. Hazards Earth Syst. Sci., 14, 473–483, https://doi.org/10.5194/nhess-14-473-2014, 2014.

Najibi, N., Perez, A. J., Arnold, W., Schwarz, A., Maendly, R., and Steinschneider, S.: (2024). A statewide, weather-regime based stochastic weather generator for process-based bottom-up climate risk assessments in California – Part II: Thermodynamic and dynamic climate change scenarios, Climate Services, 34, 100485, https://doi.org/10.1016/j.cliser.2024.100485, 2024.

NatCatSERVICE: Global Natural Catastrophe and Socioeconomic Impact Database, Munich Re, https://www.munichre.com/en/reinsurance/business/non-life/natcatservice/index.html(last access: 28 Aug 2025), 2023

Naveau, P., Huser, R., Ribereau, P. and Hannart, A.: Modeling jointly low, moderate, and heavy rainfall intensities without a threshold selection, Water Resour. Res., 52, 2753–2769, https://doi.org/10.1002/2015WR018552, 2016.

Nguyen, V. D., Merz, B., Hundecha, Y., Haberlandt, U., and Vorogushyn, S.: Comprehensive evaluation of an improved large-scale multi-site weather generator for Germany, Int. J. Climatol., 41, 4933–4956, https://doi.org/10.1002/joc.7107, 2021.

Nguyen, V. D., Vorogushyn, S., Nissen, K., Brunner, L., and Merz, B.: A non-stationary climate-informed weather generator for assessing future flood risks, Adv. Stat. Clim. Meteorol. Oceanogr., 10, 195–216, https://doi.org/10.5194/ascmo-10-195-2024, 2024.

Orlanski, I.: A Rational Subdivision of Scales for Atmospheric Processes, B. Am. Meteorol. Soc., 56, 527–530, 1975.

Philipp, A., Della-Marta, P. M., Jacobeit, J., Fereday, D. R., Jones, P. D., Moberg, A., and Wanner, H.: Long-Term Variability of Daily North Atlantic–European Pressure Patterns since 1850 Classified by Simulated Annealing Clustering, J. Climate, 20, 4065–4095, https://doi.org/10.1175/jcli4175.1, 2007.

Qin, X. and Lu, Y.: Study of Climate Change Impact on Flood Frequencies: A Combined Weather Generator and Hydrological Modeling Approach, J. Hydrometeorol., 15, 1205–1219, https://doi.org/10.1175/JHM-D-13-0126.1, 2014.

Ramos, A. M., Trigo, R. M., and Liberato, M. L. R.: Ranking of multi-day extreme precipitation events over the Iberian Peninsula, Int. J. Climatol., 37, 607–620, https://doi.org/10.1002/joc.4726, 2017.

Sairam, N., Brill, F., Sieg, T., Farrag, M., Kellermann, P., Nguyen, V. D., Lüdtke, S., Merz, B., Schröter, K., Vorogushyn, S., and Kreibich, H.: Process-Based Flood Risk Assessment for Germany, Earth's Future, 9, e2021EF002259, https://doi.org/10.1029/2021EF002259, 2021.

Serinaldi, F. and Kilsby, C. G.: Simulating daily rainfall fields over large areas for collective risk estimation, J. Hydrol., 512, 285–302, https://doi.org/10.1016/j.jhydrol.2014.02.043, 2014.

Steinschneider, S. and Brown, C.: A semiparametric multivariate, multisite weather generator with low-frequency variability for use in climate risk assessments, Water Resour. Res., 49, 7205–7220, https://doi.org/10.1002/wrcr.20528, 2013.

Swiss Re Institute: sigma: Natural catastrophes in 2023: Gearing up for today's and tomorrow's weather risks (No 1/2024), Swiss Re Ltd., Zurich, Switzerland, https://www.swissre.com/dam/jcr:c9385357-6b86-486a-9ad8-78679037c10e/2024-03-sigma1-natural-catastrophes.pdf, (last access: 28 August 2025), 2024.

https://doi.org/10.5194/nhess-25-3075-2025

Nat. Hazards Earth Syst. Sci., 25, 3075–3086, 2025

Szönyi, M., Roezer, V., Deubelli, T., Ulrich, J., MacClune, K., Laurien, F., and Norton, R.: PERC Flood event review "Bernd" https://floodresilience.net/zurich-flood-resilience-alliance/ (last access: 28 Aug 2025), 2022.

Thieken, A. H., Samprogna Mohor, G., Kreibich, H., and Müller, M.: Compound inland flood events: different pathways, different impacts and different coping options, Nat. Hazards Earth Syst. Sci., 22, 165–185, https://doi.org/10.5194/nhess-22-165-2022, 2022.

Tseng, S. C., Chen, C. J., and Senarath, S. U. S.: Evaluation of multi-site precipitation generators across scales, Int. J. Climatol., 40, 4638–4656, https://doi.org/10.1002/joc.6480, 2020.

Ullrich, S. L., Hegnauer, M., Nguyen, D. V., Merz, B., Kwadijk, J., and Vorogushyn, S.: Comparative evaluation of two types of stochastic weather generators for synthetic precipitation in the Rhine basin, J. Hydrol., 601, 126544, https://doi.org/10.1016/j.jhydrol.2021.126544, 2021.

Ulrich, J., Jurado, O. E., Peter, M., Scheibel, M., and Rust, H. W.: Estimating IDF Curves Consistently over Durations with Spatial Covariates, Water, 12, 3119, https://doi.org/10.3390/w12113119, 2020.

Ulrich, J., Ritschel, C., Mack, L., Jurado, O. E., Fauer, F. S., Detring, C., and Joedicke, S.: IDF: Estimation and Plotting of IDF Curves, R package version 2.1.2, CRAN [code], https://CRAN.R-project.org/package=IDF (last access: 22 July 2022), 2021.

Voit, P.: xWEI-Quantifying-the-extremeness-of-precipitation-across-scales - Code Repository, Version v.1.0.1, Zenodo [code], https://doi.org/10.5281/zenodo.6556463, 2022.

Voit, P. and Heistermann, M.: A new index to quantify the extremeness of precipitation across scales, Nat. Hazards Earth Syst. Sci., 22, 2791–2805, https://doi.org/10.5194/nhess-22-2791-2022, 2022.

Voit, P. and Heistermann, M.: A downward-counterfactual analysis of flash floods in Germany, Nat. Hazards Earth Syst. Sci., 24, 2147–2164, https://doi.org/10.5194/nhess-24-2147-2024, 2024.

Vorogushyn, S., Han, L., Apel, H., Nguyen, V. D., Guse, B., Guan, X., Rakovec, O., Najafi, H., Samaniego, L., and Merz, B.: It could have been much worse: spatial counterfactuals of the July 2021 flood in the Ahr Valley, Germany, Nat. Hazards Earth Syst. Sci., 25, 2007–2029, https://doi.org/10.5194/nhess-25-2007-2025, 2025.

Wilks, D. S.: Multisite generalization of a daily stochastic precipitation generation model, J. Hydrol., 210, 178–191, https://doi.org/10.1016/S0022-1694(98)00186-3, 1998.

Winter, B., Schneeberger, K., Dung, N.V., Huttenlau, M., Achleitner, S., Stötter, J., Merz, B., and Vorogushyn, S.: A continuous modelling approach for design flood estimation on sub-daily time scale, Hydrolog. Sci. J., 64, 539–554, https://doi.org/10.1080/02626667.2019.1593419, 2019.

Woo, G.: Downward Counterfactual Search for Extreme Events, Frontiers in Earth Science, 7, 340, https://doi.org/10.3389/feart.2019.00340, 2019.

Yang, L., Franzke, C. L. E., and Duan, W.: Evaluation and projections of extreme precipitation using a spatial extremes framework, Int. J. Climatol., 43, 3453–3475, https://doi.org/10.1002/joc.8038, 2023.

Zhang, X., Alexander, L., Hegerl, G. C., Jones, P., Tank, A. K., Peterson, T. C., Trewin, B., and Zwiers, F. W.: Indices for monitoring changes in extremes based on daily temperature and precipitation data, WIREs Climate Change, 2, 851–870, https://doi.org/10.1002/wcc.147, 2011.

Zhou, L., Meng, Y., Lu, C., Yin, S., and Ren, D.: A frequency-domain nonstationary multi-site rainfall generator for use in hydrological impact assessment, J. Hydrol., 585, 124770, https://doi.org/10.1016/j.jhydrol.2020.124770, 2020.